Journal of Medical Virology

WILEY

JOURNAL OF MEDICAL VIROLOGY

RESEARCH ARTICLE OPEN ACCESS

Comparing Cross-Sectional and Longitudinal Study Designs for Accurate Viral Dynamics Estimation: Insights From the NBA Cohort Data

Jihyeon Kim[1] | Hyeongki Park[2,3] | Hoong Kai Chua[4] | Yuqian Wang[4] | Shingo Iwami[3,5,6,7,8,9] | Yong Dam Jeong[3,10] | Koya Ariyoshi[11] | Po Ying Chia[4,12,13] | Barnaby E. Young[4,12,13] | Matthew E. Cove[14] | Robin N. Thompson[15] | William Hart[15] | Il Hyo Jung[10,16] | Kwang Su Kim[3,17] | Hyojung Lee[1] | Keisuke Ejima[4,12]

[1]Department of Statistics, Kyungpook National University, Daegu, South Korea | [2]School of Biomedical Convergence Engineering, Pusan National University, Yangsan, South Korea | [3]Interdisciplinary Biology Laboratory (iBLab), Division of Natural Science, Graduate School of Science, Nagoya University, Nagoya, Japan | [4]Lee Kong Chian School of Medicine, Nanyang Technological University, Singapore, Singapore | [5]Institute of Mathematics for Industry, Kyushu University, Fukuoka, Japan | [6]Institute for the Advanced Study of Human Biology (ASHBi), Kyoto University, Kyoto, Japan | [7]NEXT-Ganken Program, Japanese Foundation for Cancer Research (JFCR), Tokyo, Japan | [8]Interdisciplinary Theoretical and Mathematical Sciences Program (iTHEMS), RIKEN, Saitama, Japan | [9]Science Groove Inc., Fukuoka, Japan | [10]Institute of Mathematical Sciences, Pusan National University, Busan, South Korea | [11]School of Tropical Medicine and Global Health, Nagasaki University, Nagasaki, Japan | [12]National Center for Infectious Diseases, Singapore, Singapore | [13]Tan Tock Seng Hospital, Singapore, Singapore | [14]Department of Medicine, National University Hospital, Singapore, Singapore | [15]Mathematical Institute, University of Oxford, Oxford, UK | [16]Department of Mathematics, Pusan National University, Busan, South Korea | [17]Department of Scientific Computing, Pukyong National University, Busan, South Korea

Correspondence: Hyojung Lee (hjlee@knu.ac.kr) | Keisuke Ejima (keisuke.ejima@ntu.edu.sg)

Received: 20 September 2025 | **Revised:** 14 December 2025 | **Accepted:** 20 January 2026

Funding: New Faculty Research Grant of Pusan National University; AMED research program, Grant/Award Number: 24fk0210154h0001; Korea Health Technology R&D Project through the Korea Health Industry Development Institute (KHIDI) funded by the Ministry of Health & Welfare, Republic of Korea, Grant/Award Number: RS-2023-KH135442; National Research Foundation of Korea (NRF) grant funded by the Korean Government (MSIT), Grant/Award Numbers: NRF-2022R1A5A1033624, 2022R1C1C1006237, RS-2023-00227944; Lee Kong Chian School of Medicine startup grant, Grant/Award Number: #022487-00001; JST, PRESTO, Grant/Award Number: JPMJPR23R3

Keywords: COVID-19 | mathematical model | policy guidance | SARS-CoV-2 | viral dynamics | within-host

ABSTRACT

Viral load data provide critical insights into host-pathogen interactions and guide clinical and public health decisions. Because frequent testing is often infeasible, viral dynamics models are used to reconstruct infection trajectories, but optimal sampling strategies remain unclear. We compared two approaches for collecting SARS-CoV-2 viral load data: cross-sectional sampling (one measurement at symptom onset) and longitudinal sampling (every 3 days after onset) under constraints on the total number of tests and tests per individual. A viral dynamics model was first fitted to data from the National Basketball Association cohort, and the estimated parameters were treated as ground truth. Synthetic data were then generated under each sampling design, refitted, and evaluated for accuracy in estimating viral load over 30 days, peak viral load, peak time, and viral shedding duration. Longitudinal sampling consistently yielded lower root mean squared error and narrower one standard deviation interval than cross-sectional sampling. Peak timing and viral shedding duration were unbiased under both designs, but cross-sectional designs underestimated peak viral load and produced wider one standard deviation intervals. Coverage of viral load estimates was markedly higher for longitudinal designs (> 0.90) compared with cross-sectional ones (~0.10). Accuracy

Jihyeon Kim and Hyeongki Park contributed equally to this study as first authors.

Hyojung Lee and Keisuke Ejima contributed equally as corresponding authors.

and coverage exceeded 0.96 even with just two tests per individual, with little additional benefit from more tests. In conclusion, longitudinal sampling—despite limited data—substantially improves accuracy and precision of viral load estimation compared with cross-sectional designs. These findings highlight efficient strategies for study design and resource allocation in infectious disease research.

1 | Introduction

The coronavirus disease 2019 (COVID-19) pandemic was an unprecedented global health crisis caused by the highly contagious respiratory virus, severe acute respiratory syndrome coronavirus 2 (SARS-CoV-2). Though a relatively short period in human history, the COVID-19 pandemic has fundamentally reshaped public health policies [1–3], transformed epidemiological practices [4–6], and driven rapid advancements in vaccine and drug development [7–9]. A key cornerstone in facilitating such significant progress is the collection of vast amounts of epidemiological and clinical data. Among them, viral load data has demonstrated its versatile potential in providing valuable insights into host-pathogen dynamics [10, 11], as well as informing strategies for disease control and management [12, 13].

Viral RNA load is typically obtained from reverse transcription-quantitative polymerase chain reaction (RT-qPCR) tests based on its inverse relationship with the cycle threshold (C_t) value [14], which is the number of amplification cycles required for the viral amplicon signals to become detectable. Depending on the purpose of data collection, different study designs are used, resulting in viral load data that generally fall into one of two categories: cross-sectional or longitudinal. Cross-sectional data comprises viral load measurements collected from individuals at only a single time point. For example, samples can be taken from individuals who are seeking a clinical diagnosis, are identified as close contacts in contact tracing, or are involved in screening events as part of community surveillance. In other words, cross-sectional data are typically collected during the process of identifying infected individuals, which is useful for monitoring and predicting the epidemiological situation [15, 16]. In contrast, longitudinal data involve repeated viral load measurements collected from the same individuals at multiple time points. For example, longitudinal viral load data have been collected as a prognostic biomarker in clinical practice [17, 18].

Due to the dynamic nature of host-pathogen interactions during acute infection, viral load reflects the progression of infection over time. For viruses causing acute infection, the viral load rises exponentially during the initial phase, hits a peak, and gradually declines. Mathematical models have been used to capture this viral load trajectory over time by incorporating key biological processes of infection within a host, such as viral replication and elimination due to immune response [12, 13, 18–25]. However, even when viral dynamics models are applied appropriately, their accuracy depends on the underlying dataset. Optimal sampling strategies to improve inference remain inadequately defined. Several previous studies have shown that the viral dynamics estimation from longitudinal data enhances accuracy [26, 27]. Generally, increasing the frequency of viral load measurements per individual improves the precision of viral dynamics estimation. However, in resource-constrained settings where the total number of collectible samples is fixed, quantitative comparisons of estimation accuracy between cross-sectional and longitudinal study designs remain scarce. Therefore, it is crucial to identify the optimal balance between the number of individuals sampled and the number of measurements per individual to accurately estimate viral dynamics within a fixed resource budget. In this case, what is the minimum number of sampling points required? Would a cross-sectional study with a large study population yield results comparable to those of a longitudinal study with a smaller cohort? In a longitudinal study design, how many time points per individual are required?

In light of the above, the aims of this study are to: (1) compare the accuracy of cross-sectional and longitudinal viral load data in recapitulating the viral load dynamics, and (2) develop an optimal data collection protocol for different study designs. Addressing these research gaps is crucial to improving the design of future studies, balancing the immediate needs of public health systems with long-term scientific understanding, thus enhancing our overall response to future emerging pathogens beyond SARS-CoV-2.

2 | Methods

2.1 | Overview of the Approach

We conducted a series of simulations to assess the accuracy of SARS-CoV-2 viral dynamics estimation under cross-sectional and longitudinal study designs. First, to capture realistic viral dynamics, we fitted a mathematical model to SARS-CoV-2 viral load data collected from National Basketball Association (NBA) players, staff, and vendors [26–28]. Second, we generated synthetic viral load data using the estimated parameter distributions and following different study designs. We simulated two study designs: longitudinal (measurements every 3 days from symptom onset) and cross-sectional (a single measurement at symptom onset). Lastly, we estimated the viral trajectory from the synthetic datasets and assessed the impact of study designs on the accuracy of viral dynamics estimates.

2.2 | Viral Load Dataset

We utilized longitudinal SARS-CoV-2 viral load data collected from NBA players, staff, and vendors through anterior nares and oropharyngeal swabs between July 2020 and January 2022. This dataset is publicly available anonymized data and has been analyzed in previous studies [24, 27–30]. Most individuals were required to undergo daily testing before vaccination. After vaccination, the frequency of testing decreased, but subjects were still closely monitored. It is recognized as a valuable resource for inferring viral load dynamics, especially in the early phase of infection, due to the regular and widespread screening tests conducted. C_t values were measured twice for each measurement event using RT-qPCR tests (Roche cobas

target 1 assay) performed on combined swabs from the anterior nares and oropharynx. In our analyzes, we used the average of the two measurements. To convert C_t values to viral load, we used the equation [29]: $C_t = -3.6097 \times \log_{10}(V) + 49.5932$, where V is the viral RNA load (copies/mL). The detection limit of this dataset was $C_t = 40$ (equivalent to $10^{2.656}$ copies/mL), and the day of symptom onset was recorded for all symptomatic cases. In total, 2,678 individuals were tested, each undergoing 1 to 76 tests, with an average of 10 tests per person. Testing started up to 14 days before the first positive result, averaging 3 days prior to detection. To minimize the impact of variant differences, we focused on individuals infected with the Delta variant. Of the 327 Delta variant cases, 118 individuals with fewer than three positive (above detection limit) results were excluded, resulting in 209 individuals included in the analysis.

2.3 | SARS-CoV-2 Viral Dynamics Model

We investigated the dynamics of SARSCoV-2 viral load throughout infection using a target-cell limited model that does not reflect the effects of the immune system, as in our previous studies [12, 13, 20, 21, 25]. The system of ordinary differential equations is as follows:

$$\frac{dT(t)}{dt} = -\beta T(t)V(t), \tag{1}$$

$$\frac{dI(t)}{dt} = \beta T(t)V(t) - \delta I(t), \tag{2}$$

$$\frac{dV(t)}{dt} = pI(t) - cV(t). \tag{3}$$

The variables $T(t)$, $I(t)$, and $V(t)$ refer to the number of susceptible (uninfected) target cells, the number of virus-producing infected cells, and the number of viral particles (copies/mL) at time t since infection, respectively. The parameters β, δ, p, and c determine the rates of virus infection, death of infected cells, viral production, and viral clearance, respectively. Since c is typically much larger than δ *in vivo*, we applied a quasi-steady state assumption, where we can take, approximately, $\frac{dV(t)}{dt} = 0$, yielding the following simplified model:

$$\frac{df(t)}{dt} = -\beta f(t)V(t), \tag{4}$$

$$\frac{dV(t)}{dt} = \gamma f(t)V(t) - \delta V(t). \tag{5}$$

Here, the variable $f(t) = \frac{T(t)}{T(0)}$ is introduced, which is defined as the proportion of target cells remaining at time t, where $T(0)$ is the initial number of uninfected target cells (thus $f(0) = 1$). The parameter γ represents the maximum viral replication rate and is given by $\gamma = \frac{p\beta}{c}T(0)$. The initial condition for viral load was set as $V(0) = 10^{-2}$ (copies/ml) [12, 13].

2.4 | Model Fitting and Statistical Inference

We employed a nonlinear mixed-effects modeling (NLMEM) approach, which accounts for both a fixed effect (the population effect; shared across individuals) and random effects (capturing individual variability). This amounts to a partial pooling of the data from each individual, enabling parameter estimation even with sparse data. The parameter set for an individual i, θ_i, can be expressed as a product of θ (a fixed effect) and e^{η_i} (a random effect), where $\eta_i \sim N(0, \Omega)$ and Ω is the variance-covariance matrix of random effects. We used lognormal distributions as prior distributions for the parameters to guarantee positive valued estimates. In the NBA dataset, recorded times were specified relative to detection, rather than relative to infection. We therefore estimated the time from infection to detection, τ, along with the other model parameters. A right-truncated normal distribution was used in the likelihood function to account for left-censoring of the viral load data (i.e., when the viral load is under the detection limit) [31]. Specifically, censored data values were iteratively sampled along with individual random effects, allowing the likelihood to appropriately reflect the uncertainty introduced by censored data. Fixed-effect and random-effect parameters were estimated using the stochastic approximation expectation-maximization (SAEM) algorithm and empirical Bayes method, respectively, as implemented in MONOLIX 2023R1 [32] (https://www.lixoft.com) and the R package lixoftConnectors (to run MONOLIX on the statistical software R [https://www.r-project.org/]). To avoid convergence to a local maximum in the likelihood surface, we varied the initial parameter values multiple times and confirmed the robustness of the parameter estimates.

2.5 | Generation of Synthetic Viral Load Data Under Different Study Designs

After we obtained ground truth parameter estimates, β_{true}, γ_{true}, and δ_{true} and ground truth viral dynamics, $V_{true}(t)$, we generated synthetic viral load data that preserved the characteristics of the original NBA cohort while reflecting different study designs. The viral load of a virtual individual k at day t since infection was generated by running the model with a parameter set $(\beta_k, \gamma_k, \delta_k)$ randomly sampled from the estimated parameter distributions. We then added measurement error, $\varepsilon_k(t)$, to obtain the measured viral load of individual k at day t since infection, denoted as $V_k(t)$. The value of $\varepsilon_k(t)$ was randomly sampled from a normal distribution $N(0, \sigma^2)$, where σ was estimated by fitting a normal distribution to the residuals in the original fitting process. The data were generated for n individuals (i.e., $k \in \{1, 2, 3, ..., n\}$). Similarly to the original study of the NBA cohort, we set the detection limit to be $10^{2.6576}$ copies/mL ($C_t = 40$).

The synthetic dataset was then reduced appropriately to reflect the two different study designs (cross-sectional and longitudinal). For the cross-sectional study design, we assumed that viral load data are collected only at symptom onset. For the longitudinal study design, we assumed that viral load data are collected at multiple time points with defined intervals from symptom onset (with the first test at onset). To determine the timing of symptom onset, we simulated the incubation period (ω)—defined as the time from infection to symptom onset—assuming it follows a gamma distribution independent of the viral load trajectory: $Gamma(4.09, 1.08)$ (mean: 4.43 days) [33]. Since the relationship between viral dynamics and symptom onset has not been clearly defined, we assumed an incubation

period distribution in general cases rather than an estimated distribution specific to the NBA cohort [34–36]. We considered three study design parameters: total number of tests (m), the number of tests per person (u), and the interval between tests (s; only for longitudinal study design). For the cross-sectional study design, $u = 1$ by definition. When we analyzed different longitudinal study designs, we considered $m \in \{200, 500, 1000\}$, $s = 3$, and $u \in \{2,3,4,5,8\}$. To compare cross-sectional and longitudinal study designs fairly, we considered fixed values of the total number of tests performed, $m = n \times u$ (where n is the total number of individuals tested); in other words, when we considered a cross-sectional design, we used a larger value of n than when we considered the analogous longitudinal study design. We performed 100 simulations for each combination of study design parameters.

2.6 | Assessing the Accuracy of Viral Dynamics Estimation Under Different Study Designs

The accuracy of estimation was assessed by comparing the inferred viral dynamics using the population parameter estimates, β_{true}, γ_{true}, and δ_{true}, obtained from the synthetic viral load data against the ground truth viral dynamics, $V_{true}(t)$ (i.e., the viral dynamics according to the parameters estimated from the NBA cohort dataset). Accuracy was assessed by comparing four primary outcome metrics in each case: (1) root mean squared error (RMSE) of the estimated daily viral load over 30 days since infection (here we used the estimated viral load, thus we can compare the viral loads even when they are below the detection limit), (2) difference in peak viral load, (3) difference in the timing of peak viral load, and (4) difference in viral shedding duration (period when the viral load remains detectable) (Figure 1). The difference is evaluated by the mean and one standard deviation interval. In addition to considering viral dynamics based on the mean parameter estimates, we computed the coverage score at specific time points; namely, the proportion of simulation runs (out of 100 repetitions) for which the 95% prediction interval (PI) of the viral load estimated from the synthetic dataset includes the ground truth estimates, $V_{true}(t)$, from the mean population parameters at that particular time point. To summarize performance across different infection stages, we averaged these time-point specific coverage scores within three distinct time phases: before the peak (0–2 days after infection), around the peak (2–8 days after infection), and after the peak (8–15 days after infection). The detailed calculation formula for a single study design with 100 replications is as follows.

1. Mean RMSE of the estimated daily viral load over 30 days since infection:

   $$Mean\ RMSE = \frac{1}{100}\sum_{k=1}^{100}\left(\frac{1}{30}\sum_{t=0}^{30}(V_k(t) - \bar{V}_k)^2\right).$$

2. Mean and one standard deviation interval for peak viral load, timing of peak viral load, and viral shedding duration:

   $$[\bar{x} - sd, \bar{x} + sd],\ where\ \bar{x} = \frac{1}{100}\sum_{k=1}^{100} x_k,\ sd = \sqrt{\frac{1}{100}\sum_{k=1}^{100}(x_i - \bar{x})^2}$$

   and x is peak viral load, timing of peak viral load, or viral shedding duration.

3. Coverage score ($C(t)$):

$$C(t) = \frac{1}{100}\sum_{k=1}^{100} I(LV_k(t) \le V_{true}(t) \le UV_k(t)),$$ for $t \in$ {before the peak, around the peak, after the peak}, where $LV_k(t)$ and $UV_k(t)$ mean lower bound and upper bound of 95% PI for $V_k(t)$.

3 | Results

3.1 | Estimated Viral Load Trajectories From the NBA Cohort Data and Synthetic Data

Figure 2 shows the viral load trajectory for the NBA cohort using the estimated population parameters. The estimated population parameter values are listed in Table 1. The peak

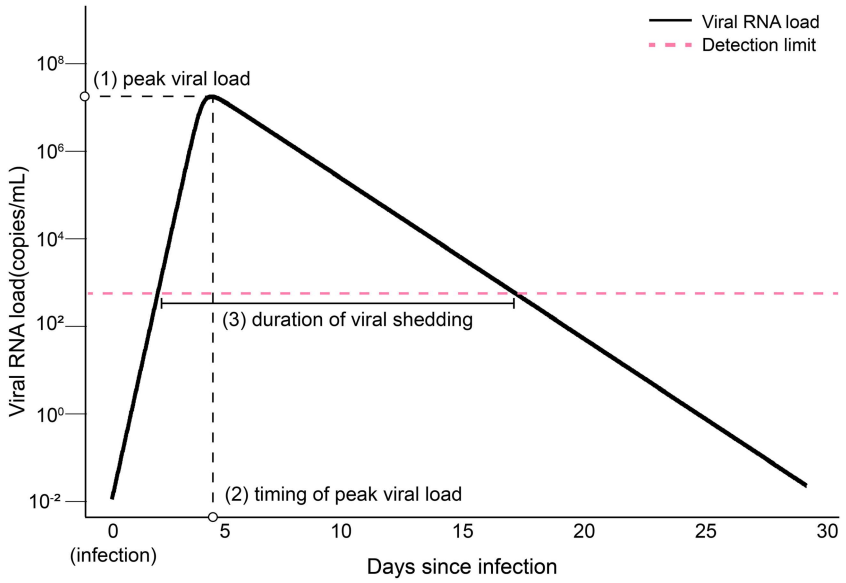

FIGURE 1 | Characteristics of the viral load trajectory used for accuracy assessment. The accuracy of the viral dynamics estimation was evaluated by comparing population estimates derived from the synthetic viral load data (under different study designs) to those obtained from the NBA cohort, which served as the ground truth. Four characteristics of the viral load trajectory were compared: (1) viral load over 30 days, (2) peak viral load, (3) timing of peak viral load, and (4) viral shedding duration. The dashed pink line represents the detection limit ($10^{2.656}$ copies/mL).

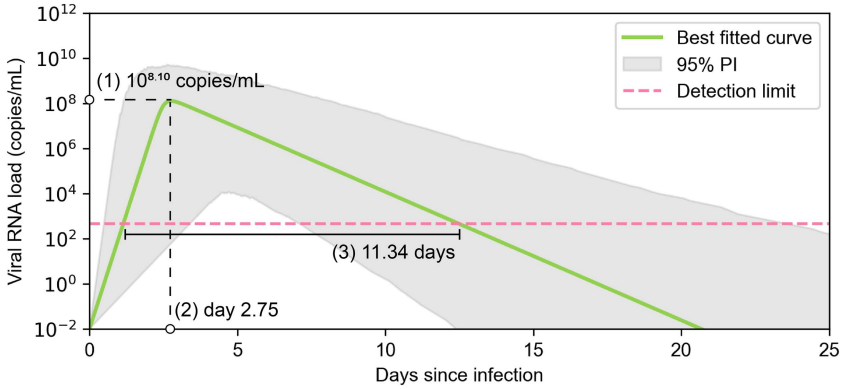

FIGURE 2 | Population viral load trajectory estimated from the NBA cohort data. The solid green line represents the best fitted viral RNA load (copies/mL) trajectory after the day of infection estimated from the NBA cohort. Three characteristics are shown: (1) peak viral load, (2) timing of peak viral load, and (3) viral shedding duration. The shaded gray area indicates the 95% prediction interval (PI) computed by using 100 parameter sets randomly sampled from the estimated distribution of the population parameters. The dashed pink line represents the detection limit ($10^{2.656}$ copies/mL).

viral load, the timing of the peak, and the duration of viral shedding were $10^{8.10}$ copies/mL, 2.75 days after infection, and 11.34 days, respectively, with the best fit parameters, which were used as the ground truth for the subsequent analyzes. Fitted viral load trajectories for a random set of individuals are shown in Supporting Information Figure S1. The model fit yielded an AIC of 5619. Convergence of all model parameters was confirmed by examining the SAEM convergence profiles (Supporting Information Figure S2). Parameter identifiability (RSE, shrinkage, and parameter correlations) and robustness (bootstrap analyzes) were assessed in Supporting Information Table S1 and Supporting Information Table S2, respectively, demonstrating stable and reliable estimation.

Next, we generated synthetic data by utilizing the distributions of parameters estimated from the NBA dataset (see Methods for details). Individual-level viral dynamics trajectories were simulated by randomly sampling parameters, and synthetic data were then generated according to the study design. Based on the simulated data, population-level parameters were re-estimated. This process of data generation and parameter estimation was repeated 100 times for each study design scenario. Specifically, we performed simulations by fixing the total number of data points at 200, 500, and 1000, while varying the number of test measurements per individual to 1 (cross-sectional design), 2, 3, 4, 5 or 8 (longitudinal design). Focusing on the designs with one, two, and three test measurements per individual, we analyzed the distributions of 100 estimated population-level viral dynamics trajectories (Figure 3). A key aspect of this setup is that the total number of data points was held constant: for instance, with 200 total data points, the cross-sectional design would require 200 participants, whereas the longitudinal design with two test measurements per person would require only 100 participants.

In the cross-sectional design, the estimated dynamics deviated from the ground truth during both the early and late phases of infection (Figure 3A). Although increasing the total number of data points reduced the variability among estimated trajectories, it did not substantially improve the accuracy relative to the ground truth. Indeed, in scenarios with 200, 500, and 1000 total data points, the RMSE showed minimal differences at 2.22, 2.33, and 2.35, respectively (Figure 3A). In contrast, under the longitudinal design, testing each individual twice allowed for reasonably accurate estimation during the early phase of infection, though estimates during the later phase remained unstable (Figure 3B). With three tests per person, however, the estimated trajectories closely aligned with the ground truth throughout both phases (Figure 3C). Notably, in longitudinal designs, increasing the total number of data points not only reduced trajectory variability but also improved overall accuracy, as reflected in the RMSE values (Figure 3B,C). For the 200 data points, the RMSEs were 1.93 and 1.38 with two and three measurements per person. But as the number of data points increased to 500 and 1000, the RMSEs decreased to 1.50 and 0.68, and to 0.67, and 0.43, respectively. This suggests that the improvement in estimation accuracy resulting from additional total data points is more pronounced in longitudinal designs compared to cross-sectional designs.

In addition, for the scenarios in which each individual was tested four, five, or eight times, the overall results were largely similar to those observed with three tests per individual (Supporting Information Figure S3). Interestingly, the mean RMSE increased instead when each individual was tested 8 times. This may be attributable to right censoring due to the detection limit of viral load in the late phases of infection, resulting in a loss of informative observations. In other words, when the total number of data points is fixed, allocating too many test measurements per individual may result in a reduced number of participants, with the loss in population coverage outweighing the benefits of increased data density per person.

3.2 | Comparison of Study Designs

To conduct a more detailed assessment of the viral dynamics estimated under each study design, we evaluated three features to quantitatively describe the viral dynamics: peak viral load, timing of the peak, and viral shedding duration. For each metric, the ground truth values were $10^{8.10}$ copies/mL, 2.75 days after infection, and 11.34 days. Figure 4 illustrates the mean and one standard deviation interval of the three metrics of the accuracy of the estimation under different study designs (i.e., mean [mean − SD, mean + SD]). Under a cross-sectional study design, the mean ± standard deviation (i.e., mean ± SD) of peak

TABLE 1 | Estimated model parameters for SARS-CoV-2 delta variant from the NBA cohort data.

Parameter[a]	Maximum rate constant for viral replication	Rate constant for virus infection	Death rate of infected cells	Time from infection to detection
Symbol	γ	β	δ	τ
Unit	day^{-1}	$(copies/mL)^{-1}\ day^{-1}$	day^{-1}	days
Fixed effect (population parameter)[b]	10.73 (0.52)	0.0053×10^{-5} (0.0013)	1.31 (0.051)	2.19 (0.087)
Standard deviation of random effect[c]	0.42 (0.036)	2.37 (0.19)	0.33 (0.028)	0.1 (0.028)
Standard deviation of the residual error[c]		1.37 (0.035)		

[a]Numbers in parentheses are the standard error.
[b]Lognormal distributions were assumed.
[c]Normal distributions were assumed with mean 0.

viral load was 7.36 ± 0.26, 7.26 ± 0.17, and 7.27 ± 0.13, showing a tendency to be underestimated regardless of the number of test points and the one standard deviation interval does not include the ground truth value (Figure 4A). Under a longitudinal study design, the estimated peak viral load is close to the ground truth, and the one standard deviation interval includes the ground truth. The differences with ground truth were under 0.2 for all data points for each estimated peak viral load mean according to the number of tests per person. For the estimation of the timing of the peak, the one standard deviation intervals cover the ground truth regardless of the study designs (Figure 4B). Interestingly, the cross-sectional study yielded wide one standard deviation intervals of nearly 4, with a standard deviation close to 2, resulting in less stability of estimation. Whereas the longitudinal study showed more precision, with a difference between the ground truth and the mean estimated timing of peak viral load less than 1 and a standard deviation below 2, even if the number of points per individual was as small as two. An increase in the number of tests per individual (with the same total number of tests) in the longitudinal study had minimal impact on the estimation. Even when the total data points was 200, the mean estimates differed by 0.66 or less from the ground truth as the number of tests per person increased as 2, 3, 4, 5, and 8: 2.09, 2.15, 2.36, 2.89, and 2.11. Furthermore, as the total data points increased, these differences became smaller. Similar to the estimation of the timing to the peak viral load, the one standard deviation interval for the estimated viral shedding duration included the ground truth across all study designs (Figure 4C). However, in both the cross-sectional design and the longitudinal design with only two measurements per individual, the one standard deviation intervals were particularly wide at values close to 5 (i.e., approximately 2.5 standard deviation) for 200 and 500 total data points, indicating lower estimation stability. This suggests that at least three test measurements per individual are necessary to reliably estimate the viral shedding duration. With three tests, the mean $\pm$ SD of the estimated viral shedding duration approached the ground truth as the total data points increased, becoming 12.13 ± 1.66, 11.85 ± 0.78, and 11.64 ± 0.40, while the standard deviation decreased. Thus, within the same study design, the one standard deviation interval became narrower (i.e., more precise estimates) as the number of data points increased in all the accuracy metrics.

In addition, a comparative analysis was performed on the estimated parameters for each study design (Supporting Information Figure S4). Overall, the results showed a pattern similar to those observed in the analysis of features of viral dynamics: as the total number of data points increased, the credible intervals shortened, and the difference between the mean of estimates and ground truth decreased, improving estimation stability. The longitudinal designs, which included at least three test measurements per individual, demonstrated both high precision and stability. Notably, in the cross-sectional design, the parameter γ (representing the virus production rate from infected cells) tended to be significantly underestimated. Given the close association between γ and peak viral load, this finding is consistent with the underestimation of peak viral load observed in the cross-sectional design.

In the study of cross-sectional data sampling, we only estimated population-level parameters, focusing exclusively on the fixed

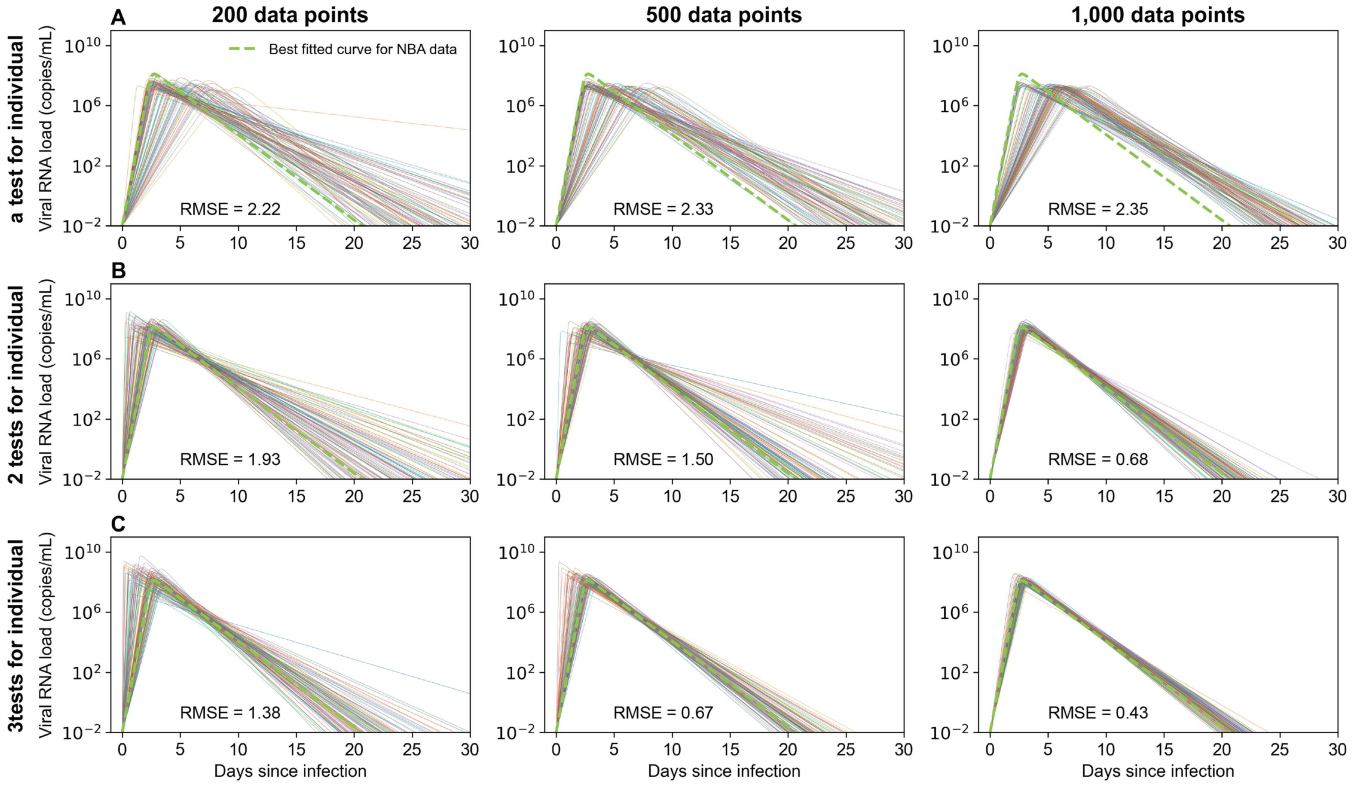

FIGURE 3 | Population viral trajectory estimated under different study designs. (A) The solid lines are the population viral load trajectories estimated from the synthetic data under cross-sectional study designs with different numbers of data points (200, 500, and 1,000). The dashed green line represents the best fitted viral RNA load (copies/mL) after the day of infection estimated from the NBA cohort (i.e., the ground truth). The root mean squared error (RMSE) of the viral dynamics over 30 days is indicated in text. Simulations were repeated 100 times. (B) The same as A, but under the longitudinal study designs (two tests for each individual). (C) The same as B, but three tests for each individual.

effect of the model (see Methods for details). This is because, in cross-sectional settings with only a single observation per subject, random-effects components are generally not identifiable, as they are confounded with the residual error. In practice, estimation of random effects typically requires repeated measurements per subject [37, 38].

Nevertheless, we examined whether random effect estimation can improve the estimation accuracy in cross-sectional data sampling to examine how the inclusion or exclusion of random effects might influence the estimation results (Supporting Information Figure S5). The results showed a slight improvement in the accuracy of the estimated peak viral load, although it still tended to be underestimated. We presumed this is because it is difficult to determine whether a single data point was observed before or after the peak per individual. For example, if an observation is interpreted as before the peak, the increasing slope becomes gentle, which can result in an underestimate of the parameter γ(gamma). In addition, the accuracy of the estimated timing of peak viral load improved significantly, while the accuracy of estimated viral shedding duration was rather lowered. Overall, in cross-sectional data sampling, it was difficult to obtain the accuracy of estimation as much as the longitudinal data sampling even considering the random effect.

We employed a target-cell limited model, but more complex models incorporating the adaptive immune response might be necessary to biologically reasonably explain the dynamics. Therefore, we simulated using the model considering the immune response presented by the previous study [18]. As a result of simulation, we confirmed the superiority of the longitudinal study, which is consistent with those from the target-cell limited model. Also, the increasing number of estimated parameters makes it difficult to obtain reasonable estimates, and considering that more complex models may require information beyond viral titers [34]. This supports the validity of our study's approach using a simple model. Furthermore, several studies have shown that immune response models didn't improve the estimation results of a target-cell limited model, and suggested that immune responses are implicitly incorporated into the model parameters such as the infection rate and the mortality rate of infected cells [35, 36].

As secondary outcomes, the mean coverage score was computed for different time phases: before peak (0–2 days after infection), peak (2–8 days after infection), and after peak (8–15 days after infection). Each phase's score represents the mean proportion, across the time points within that phase, of simulation runs (out of 100) where the estimated 95% PI included the ground truth viral load. The full score (i.e., 1) suggests that the viral load estimated from the synthetic data covers the ground truth over the period. Therefore, the closer the coverage score is to 1, the more similar the viral dynamics estimate over time in the corresponding study design is to the ground truth. Supporting Information Figure S6 presents the boxplot showing the distribution of these 100 phase-averaged coverage scores obtained from the 100 repetitions for each study design. Under cross-sectional study designs, the median phase-averaged coverage

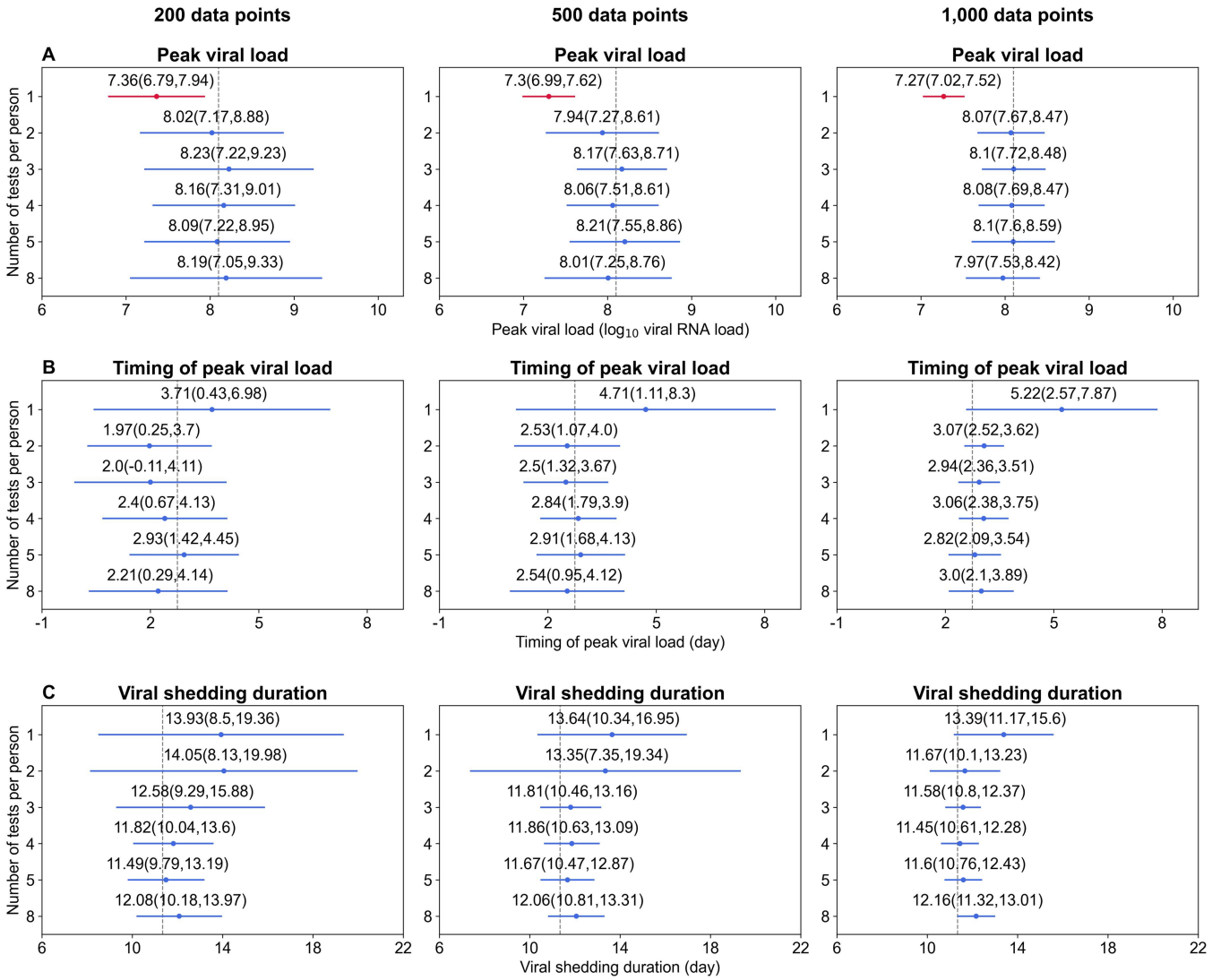

FIGURE 4 | Accuracy on viral dynamics estimation under different study designs. (A) The value of the peak viral load under different numbers of tests per person (1–5 and 8) and the number of data points (200, 500, 1000). (B) The same as A, but the difference in the timing of peak viral load. (C) The same as B, but the difference in the viral shedding duration. Each point represents the mean estimate, the solid lines are the one standard deviation of the mean, and the gray vertical dashed lines are ground truth values. Red indicates when the one standard deviation of the mean does not include the ground truth, while blue indicates when it does.

score is around 0.10 across all the three time phases, regardless of the total number of data points. Under longitudinal study designs, the median coverage score consistently exceeds 0.90. Within the same time phase and the same study designs, the coverage score slightly increases as the total number of data points increases. Only a limited difference was observed under different numbers of tests per person.

4 | Discussion

Viral load data have provided valuable insights in both clinical and public health contexts. Since such data are typically collected in a discrete manner, various analytical approaches have been employed to extract meaningful information, one of which involves the use of mathematical modeling. The main advantage of mathematical modeling is that it can reconstruct viral load trajectories even from a limited number of data points. However, the accuracy of such estimates depends on the data collection strategy and sampling frequency. While richer datasets increase precision, excessive sampling may create unnecessary burdens. Thus, it is important to consider approaches that minimize data collection effort while still maintaining reliable estimation. However, quantitative discussions on optimal data collection strategies for accurately capturing viral dynamics have been limited. Two representative data sampling designs are cross-sectional and longitudinal designs. While individual-level viral dynamics analysis requires longitudinal data, average-level dynamics (population viral dynamics) can, in principle, be estimated from both. Notably, cross-sectional designs offer the advantage of rapid and easy data collection, making them particularly useful in urgent public health situations such as the early phase of a pandemic. Nevertheless, few studies have quantitatively compared the accuracy of viral dynamics estimation between these two designs.

A key contribution of this study is the quantitative comparison and analysis of the accuracy and efficiency of estimating the

average viral dynamics of SARS-CoV-2 Delta variant between cross-sectional and longitudinal designs using mathematical modeling, under the condition of a fixed total number of measurements (i.e., a fixed resource budget). While previous studies often focused on the merits of individual designs, our work directly addresses the practical challenge of optimizing resource allocation in settings with limited resources. Our results showed that, even when estimating population viral dynamics, the longitudinal design provided more accurate results than the cross-sectional design. In particular, the cross-sectional approach exhibited a systematic bias, consistently underestimating the peak viral load even when the total number of data points was increased. This is expected because only fixed effects were estimated without considering random effects.

Moreover, simulation results varying the number of measurements per individual within the longitudinal design revealed that even with only two measurements per person, high estimation accuracy could be achieved. With three measurements, key indicators of viral dynamics could be estimated reliably. This highlights a substantial gain in efficiency. For example, with a total budget of 200 tests, a longitudinal design requiring three tests per person only needs about 67 participants to achieve stable results. This is in strong contrast to the 200 participants needed for a cross-sectional study. These findings offer practical insights for optimizing study design. We demonstrate that an efficient longitudinal strategy maximizes accuracy in real-world research settings, where data collection resources are often limited.

This is not the first study focusing on the accuracy of viral dynamics estimation. For example, Zitzmann et al. found that model parameters cannot be estimated well if viral load data at the initial phase of infection before the peak are completely missing [30]. Chua et al. demonstrated that more tests per person, longer test intervals, and larger patient samples are key to estimate the viral trajectory accurately, and suggested an optimal cohort study design (interval between tests and number of tests per person) to minimize the length of follow up [25]. Note that both studies have focused only on longitudinal data. In this study, we extended this approach to further compare cross-sectional data and longitudinal data.

There are a few strengths in this study. First, the synthetic data were generated based on longitudinal viral load data from the NBA cohort, which included early-phase measurements—even before symptom onset or diagnosis. As demonstrated in this study, longitudinal data are critical for accurate estimation of viral dynamics model parameters, and the NBA dataset uniquely captures the early phase of infection. Prior work by Zitzmann et al. has also shown that early-phase viral load data are essential for reliable parameter estimation. Therefore, the NBA cohort provides an ideal dataset for quantifying viral load dynamics. Second, by using the simulation approach, we could evaluate the accuracy of the viral load estimation under various situations. For example, the accuracy was assessed on a larger number of individuals than originally observed in the NBA data. Third, an effort was made to balance the effectiveness of the estimates against the available resources by comparing two study designs with fixed total data points. Longitudinal studies require a significant participant burden due to repeated testing and high cost of testing and follow-up management. However, they can effectively track individual changes, even with a small sample size. Conversely, cross-sectional studies involve lower individual burden and costs, but require a much larger sample size to achieve a comparable level of information to longitudinal studies. Therefore, when designing a study, it is important to consider the trade-off between high resource and burden for individuals and the need for a large sample size.

Our study provides practical implications for data collection strategies in resource-limited settings. Our findings indicate that, whenever feasible, longitudinal designs are preferable to cross-sectional ones for the estimation of viral dynamics. Nevertheless, in certain circumstances—such as when rapid response is required or when study design choices are constrained—cross-sectional sampling may be the only feasible option. In addition, cross-sectional designs are generally easier to implement for data collection than longitudinal designs. In such cases, our results can serve as a reference to anticipate the degree of bias that may arise when relying solely on cross-sectional data.

At the same time, our analyzes suggest that excessively dense sampling within longitudinal designs may represent inefficient use of resources. In particular, as demonstrated in our results, approximately three measurements per individual are sufficient to capture viral dynamics with high accuracy. This finding implies that, under constrained resources, clinical trials could enroll more participants while still maintaining robust inference. Moreover, reducing the number of measurements per participant can also shorten the overall data collection schedule. This consideration is especially relevant in outbreak settings, where timely characterization of viral dynamics is critical, and where accelerated acquisition of key information provides substantial practical advantages.

However, there are a few limitations in this study. First, our study focused exclusively on viral load data from individuals infected with the Delta variant. Then, the generalizability of the proposed optimal testing strategies to other variants, such as Omicron, may be limited. Nevertheless, a key contribution of the study is the presentation of a methodology for comparing the efficiency and accuracy of different sampling strategies. This methodological framework has the potential to be adapted and applied to investigate viral dynamics and optimize testing protocols for emerging variants or other infectious diseases. Further limitation involves the NBA cohort's limited demographic diversity, predominantly young males. Of the 209 Delta cases that were analyzed, 187 were under 50 years of age. Therefore, it is important to be careful when applying research findings to the whole population. Second, the findings of this study are specific to the methodological choices we adopted, including the parameter estimation approach. For parameter estimation, we adopted a nonlinear mixed-effects modeling (NLMEM) framework. Although this approach is widely used and robust, it is not the only possible method. These considerations indicate that our results may reflect not only the intrinsic differences between cross-sectional and longitudinal designs but also the influence of the methodological framework applied here. Third, although various indicators have been used to evaluate estimation accuracy, it is necessary to carefully determine which indicators are more important depending on the actual purpose of model fitting. For example, from an epidemiological/clinical point of view, the length of viral shedding might be most

important, as it has been used as one of the major endpoints in clinical studies and isolation guidelines [39]. Fourth, the assumption in the data collection process could be revisited. For example, we assumed the viral tests are triggered by symptom onset. However, there is a delay between symptom onset and diagnosis (thus viral tests) [40, 41]. COVID-19 epidemiological studies found that symptomatic individuals get tested (and diagnosed) on average 2.9 (range: 1-5) days after symptom onset [41]. Further, those people could be identified by screening tests (i.e., could be triggered by contact tracing) before symptom onset. Fifth, the viral load dynamics and the incubation period were treated independently when generating synthetic viral load data. This setting may limit the re-estimation process to accurately capture the ground truth. Although there may be an association between viral dynamics and the incubation period, the relationship is unclear. Individual variation is also substantial, and evidence is insufficient to define this relationship within the model. Ke et al. and Bae et al. suggested the relationship was not significant [42, 43]. Hay et al., like our study, considered the incubation period to be a separate distribution [27]. Lastly, we have not considered fully asymptomatic patients. However, we emphasize that our simulation framework is flexible enough to revisit those different assumptions.

In conclusion, our study underscores the critical importance of data collection design for accurately estimating viral load trajectories and key viral dynamics metrics. Our results demonstrate that, regardless of the total number of data points collected, longitudinal designs are consistently preferable for reliable inference of viral dynamics. Conversely, in situations where cross-sectional designs are unavoidable, our findings suggest that information on potential biases should be taken into account to aid the interpretation of the estimation results.

Author Contributions

Conceived and designed the study: Hyeongki Park, Hyojung Lee, Keisuke Ejima. Obtained and analyzed the data: Jihyeon Kim, Hyeongki Park, Hoong Kai Chua, Yuqian Wang, Hyojung Lee, Keisuke Ejima. Wrote the article: Jihyeon Kim, Hyeongki Park, Hoong Kai Chua, Yuqian Wang, Yong Dam Jeong, Po Ying Chia, Robin N. Thompson, Hyojung Lee, Keisuke Ejima. All authors read and approved the final article.

Acknowledgments

This study was supported in part by a New Faculty Research Grant of Pusan National University, 2025 (to H.P.); the AMED research program 24fk0210154h0001 (to H.P.); a grant of the Korea Health Technology R&D Project through the Korea Health Industry Development Institute (KHIDI), funded by the Ministry of Health & Welfare, Republic of Korea (RS-2023-KH135442) (to H.P.); the National Research Foundation of Korea (NRF) grant funded by the Korean Government (MSIT) (NRF-2022R1A5A1033624, NRF-2022R1C1C1006237, RS-2023-00227944) (to H.L.); a Lee Kong Chian School of Medicine startup grant (LKCMedicine-SUG, #022487-00001) (to K.E.); and JST, PRESTO (JPMJPR23R3) (to K.E.). This study does not necessarily represent the views of the funding agencies listed above.

Conflicts of Interest

The authors declare no conflicts of interest.

Data Availability Statement

The data that support the findings of this study are available in Reference [27] at https://doi.org/10.7554/elife.81849, reference [27]. These data were derived from the following resources available in the public domain: Quantifying the impact of immune history and variant on SARS, https://doi.org/10.7554/elife.81849.

Data that support the findings of this study are in the original study [27–29]. The preprocessed data used in this study is available on Github at https://github.com/modeling-computation/Virusmodel.

All analyzes were performed with the statistical computing software R (version 4.3.3) (https://www.r-project.org/). The analysis using nonlinear mixed effect models was performed on Monolix 2023R1 (https://www.lixoft.com/). The computational codes used in this study can be found on Github at https://github.com/modeling-computation/Virusmodel.

References

1. T. J. Bollyky, E. N. Hulland, R. M. Barber, et al., "Pandemic Preparedness and COVID-19: An Exploratory Analysis of Infection and Fatality Rates, and Contextual Factors Associated With Preparedness in 177 Countries, From Jan 1, 2020, to Sept 30, 2021," *Lancet* 399, no. 10334 (2022): 1489–1512, https://doi.org/10.1016/S0140-6736(22)00172-6.

2. A. Lison, N. Banholzer, M. Sharma, et al., "Effectiveness Assessment of Non-Pharmaceutical Interventions: Lessons Learned From the COVID-19 Pandemic," *Lancet Public Health* 8, no. 4 (2023): e311–e317, https://doi.org/10.1016/S2468-2667(23)00046-4.

3. T. R. Frieden, C. T. Lee, M. Lamorde, M. Nielsen, A. McClelland, and V. Tangcharoensathien, "The Road to Achieving Epidemic-Ready Primary Health Care," *Lancet Public Health* 8, no. 5 (2023): e383–e390, https://doi.org/10.1016/S2468-2667(23)00060-9.

4. A. Q. Chua, M. M. J. Tan, M. Verma, et al., "Health System Resilience in Managing the COVID-19 Pandemic: Lessons From Singapore," *BMJ Global Health* 5, no. 9 (2020): e003317, https://doi.org/10.1136/bmjgh-2020-003317.

5. R. W. Peeling, D. Boeras, A. Wilder-Smith, A. Sall, and J. Nkengasong, "Need for Sustainable Biobanking Networks for COVID-19 and Other Diseases of Epidemic Potential," *Lancet Infectious Diseases* 20, no. 10 (2020): e268–e273, https://doi.org/10.1016/S1473-3099(20)30461-8.

6. R. Badker, K. Miller, C. Pardee, et al., "Challenges in Reported COVID-19 Data: Best Practices and Recommendations for Future Epidemics," *BMJ Global Health* 6, no. 5 (2021): e005542, https://doi.org/10.1136/bmjgh-2021-005542.

7. F. S. Collins and P. Stoffels, "Accelerating COVID-19 Therapeutic Interventions and Vaccines (ACTIV): An Unprecedented Partnership for Unprecedented Times," *Journal of the American Medical Association* 323, no. 24 (2020): 2455–2457, https://doi.org/10.1001/jama.2020.8920.

8. J. J. H. Park, R. Mogg, G. E. Smith, et al., "How COVID-19 Has Fundamentally Changed Clinical Research in Global Health," *Lancet Global Health* 9, no. 5 (2021): e711–e720, https://doi.org/10.1016/S2214-109X(20)30542-8.

9. A. Von Delft, M. D. Hall, A. D. Kwong, et al., "Accelerating Antiviral Drug Discovery: Lessons From COVID-19," *Nature Reviews Drug Discovery* 22, no. 7 (2023): 585–603, https://doi.org/10.1038/s41573-023-00692-8.

10. O. Puhach, B. Meyer, and I. Eckerle, "SARS-CoV-2 Viral Load and Shedding Kinetics," *Nature Reviews Microbiology* 21, no. 3 (2023): 147–161, https://doi.org/10.1038/s41579-022-00822-w.

11. E. Normandin, M. Rudy, N. Barkas, et al., "High-Depth Sequencing Characterization of Viral Dynamics Across Tissues in Fatal COVID-19 Reveals Compartmentalized Infection," *Nature Communications* 14, no. 1 (2023): 574, https://doi.org/10.1038/s41467-022-34256-y.

12. Y. D. Jeong, K. Ejima, K. S. Kim, et al., "Revisiting the Guidelines for Ending Isolation for COVID-19 Patients," *eLife* 10 (2021): e69340, https://doi.org/10.7554/eLife.69340.

13. Y. D. Jeong, K. Ejima, K. S. Kim, et al., "Designing Isolation Guidelines for COVID-19 Patients With Rapid Antigen Tests," *Nature Communications* 13, no. 1 (2022): 4910, https://doi.org/10.1038/s41467-022-32663-9.

14. M. S. Han, J. H. Byun, Y. Cho, and J. H. Rim, "RT-PCR for SARS-CoV-2: Quantitative Versus Qualitative," *Lancet Infectious Diseases* 21, no. 2 (2021): 165, https://doi.org/10.1016/S1473-3099(20)30424-2.

15. B. Cleary, J. A. Hay, B. Blumenstiel, et al., "Using Viral Load and Epidemic Dynamics to Optimize Pooled Testing in Resource-Constrained Settings," *Science Translational Medicine* 13, no. 589 (2021): eabf1568, https://doi.org/10.1126/scitranslmed.abf1568.

16. J. A. Hay, L. Kennedy-Shaffer, S. Kanjilal, et al., "Estimating Epidemiologic Dynamics From Cross-Sectional Viral Load Distributions," *Science* 373, no. 6552 (2021): eabh0635, https://doi.org/10.1126/science.abh0635.

17. B. Killingley, A. J. Mann, M. Kalinova, et al., "Safety, Tolerability and Viral Kinetics During SARS-CoV-2 Human Challenge in Young Adults," *Nature Medicine* 28, no. 5 (2022): 1031–1041, https://doi.org/10.1038/s41591-022-01780-9.

18. N. Néant, G. Lingas, Q. Le Hingrat, et al., "Modeling SARS-CoV-2 Viral Kinetics and Association With Mortality in Hospitalized Patients From the French COVID Cohort," *Proceedings of the National Academy of Sciences* 118, no. 8 (2021): e2017962118, https://doi.org/10.1073/pnas.2017962118.

19. R. Ke, P. P. Martinez, R. L. Smith, et al., "Daily Longitudinal Sampling of SARS-CoV-2 Infection Reveals Substantial Heterogeneity in Infectiousness," *Nature Microbiology* 7, no. 5 (2022): 640–652, https://doi.org/10.1038/s41564-022-01105-z.

20. S. Iwanami, K. Ejima, K. S. Kim, et al., "Detection of Significant Antiviral Drug Effects on COVID-19 With Reasonable Sample Sizes in Randomized Controlled Trials: A Modeling Study," *PLoS Medicine* 18, no. 7 (2021): e1003660, https://doi.org/10.1371/journal.pmed.1003660.

21. K. S. Kim, S. Iwanami, T. Oda, et al., "Incomplete Antiviral Treatment May Induce Longer Durations of Viral Shedding During SARS-CoV-2 Infection," *Life Science Alliance* 4, no. 10 (2021): e202101049, https://doi.org/10.26508/lsa.202101049.

22. M. W. Tan, A. J. N. Anelone, A. T. Tay, et al., "Differences in Virus and Immune Dynamics for SARS-CoV-2 Delta and Omicron Infections by Age and Vaccination Histories," *BMC Infectious Diseases* 24, no. 1 (2024): 654, https://doi.org/10.1186/s12879-024-09572-x.

23. S. Esmaeili, K. Owens, J. Wagoner, S. J. Polyak, J. M. White, and J. T. Schiffer, "A Unifying Model to Explain Frequent SARS-CoV-2 Rebound After Nirmatrelvir Treatment and Limited Prophylactic Efficacy," *Nature Communications* 15, no. 1 (2024): 5478, https://doi.org/10.1038/s41467-024-49458-9.

24. K. Owens, S. Esmaeili, and J. T. Schiffer, "Heterogeneous SARS-CoV-2 Kinetics Due to Variable Timing and Intensity of Immune Responses," *JCI Insight* 9, no. 9 (2024): e176286, https://doi.org/10.1172/jci.insight.176286.

25. H. K. Chua, A. Singh, Y. Wang, et al., "Defining the Critical Requisites for Accurate Simulation of SARS-CoV-2 Viral Dynamics: Patient Characteristics and Data Collection Protocol," *Journal of Medical Virology* 97, no. 1 (2025): e70174, https://doi.org/10.1002/jmv.70174.

26. A. Marc, M. Kerioui, F. Blanquart, et al., "Quantifying the Relationship Between SARS-CoV-2 Viral Load and Infectiousness," *eLife* 10 (2021): e69302, https://doi.org/10.7554/elife.69302.

27. J. A. Hay, S. M. Kissler, J. R. Fauver, et al., "Quantifying the Impact of Immune History and Variant on SARS-CoV-2 Viral Kinetics and Infection Rebound: A Retrospective Cohort Study," *eLife* 11 (2022): e81849, https://doi.org/10.7554/elife.81849.

28. S. M. Kissler, J. R. Fauver, C. Mack, et al., "Viral Dynamics of Acute SARS-CoV-2 Infection and Applications to Diagnostic and Public Health Strategies," *PLoS Biology* 19, no. 7 (2021): e3001333, https://doi.org/10.1371/journal.pbio.3001333.

29. S. M. Kissler, J. R. Fauver, C. Mack, et al., "Viral Dynamics of SARS-CoV-2 Variants in Vaccinated and Unvaccinated Persons," *New England Journal of Medicine* 385, no. 26 (2021): 2489–2491, https://doi.org/10.1056/nejmc2102507.

30. C. Zitzmann, R. Ke, R. M. Ribeiro, and A. S. Perelson, "How Robust are Estimates of Key Parameters in Standard Viral Dynamic Models?," *PLoS Computational Biology* 20, no. 4 (2024): e1011437, https://doi.org/10.1371/journal.pcbi.1011437.

31. A. Samson, M. Lavielle, and F. Mentré, "Extension of the SAEM Algorithm to Left-Censored Data in Nonlinear Mixed-Effects Model: Application to HIV Dynamics Model," *Computational Statistics and Data Analysis* 51, no. 3 (2006): 1562–1574, https://doi.org/10.1016/j.csda.2006.05.007.

32. M. Lavielle, *Mixed Effects Models for the Population Approach: Models, Tasks, Methods and Tools* (CRC Press, 2014), 384.

33. S. Galmiche, T. Cortier, T. Charmet, et al., "SARS-CoV-2 Incubation Period Across Variants of Concern, Individual Factors, and Circumstances of Infection in France: A Case Series Analysis From the ComCor Study," *Lancet Microbe* 4, no. 6 (2023): e409–e417, https://doi.org/10.1016/s2666-5247(23)00005-8.

34. B. N. Williamson, F. Feldmann, B. Schwarz, et al., "Clinical Benefit of Remdesivir in Rhesus Macaques Infected With SARS-CoV-2," *Nature* 585, no. 7824 (2020): 273–276, https://doi.org/10.1038/s41586-020-2423-5.

35. A. Gonçalves, J. Bertrand, R. Ke, et al., "Timing of Antiviral Treatment Initiation Is Critical to Reduce SARS-CoV-2 Viral Load," *CPT: Pharmacometrics and Systems Pharmacology* 9, no. 9 (2020): 509–514, https://doi.org/10.1002/psp4.12543.

36. K. S. Kim, K. Ejima, S. Iwanami, et al., "A Quantitative Model Used to Compare Within-Host SARS-CoV-2, MERS-CoV, and SARS-CoV Dynamics Provides Insights Into the Pathogenesis and Treatment of SARS-CoV-2," *PLoS Biology* 19, no. 3 (2021): e3001128, https://doi.org/10.1371/journal.pbio.3001128.

37. N. M. Laird and J. H. Ware, "Random-Effects Models for Longitudinal Data," *Biometrics* 38 (1982): 963–974, https://doi.org/10.2307/2529876.

38. M. J. Lindstrom and D. M. Bates, "Nonlinear Mixed Effects Models for Repeated Measures Data," *Biometrics* 46 (1990): 673–687, https://doi.org/10.2307/2532087.

39. J. J. A. Van Kampen, D. A. M. C. van de Vijver, P. L. A. Fraaij, et al., "Duration and Key Determinants of Infectious Virus Shedding in Hospitalized Patients With Coronavirus Disease-2019 (COVID-19)," *Nature Communications* 12, no. 1 (2021): 267, https://doi.org/10.1038/s41467-020-20568-4.

40. X. Rong, L. Yang, H. Chu, and M. Fan, "Effect of Delay in Diagnosis on Transmission of COVID-19," *Mathematical Biosciences and Engineering* 17, no. 3 (2020): 2725–2740, https://doi.org/10.3934/mbe.2020149.

41. K. Mellou, S. Sapounas, I. Panagoulias, et al., "Time Lag Between COVID-19 Diagnosis and Symptoms Onset for Different Population Groups: Evidence That Self-Testing in Schools was Associated With Timely Diagnosis Among Children," *Life* 12, no. 9 (2022): 1305, https://doi.org/10.3390/life12091305.

42. R. Ke, C. Zitzmann, D. D. Ho, R. M. Ribeiro, and A. S. Perelson, "In Vivo Kinetics of SARS-CoV-2 Infection and Its Relationship With a Person's Infectiousness," *Proceedings of the National Academy of*

Sciences 118, no. 49 (2021): e2111477118, https://doi.org/10.1073/pnas.2111477118.

43. S. Bae, J. Y. Kim, S. Y. Lim, et al., "Dynamics of Viral Shedding and Symptoms in Patients With Asymptomatic or Mild COVID-19," *Viruses* 13, no. 11 (2021): 2133, https://doi.org/10.3390/v13112133.

Supporting Information

Additional supporting information can be found online in the Supporting Information section.
Supplementary Materials.